ADVANCED FUNCTIONAL MATERIALS
www.afm-journal.de



# The Exfoliation of Graphene in Liquids by Electrochemical, Chemical, and Sonication-Assisted Techniques: A Nanoscale Study

*Zhen Yuan Xia, Sergio Pezzini, Emanuele Treossi, Giuliano Giambastiani, Franco Corticelli, Vittorio Morandi, Alberto Zanelli, Vittorio Bellani, and Vincenzo Palermo**

**The different exfoliation routes of graphite to produce graphene by sonication in solvent, chemical oxidation and electrochemical oxidation are compared. The exfoliation process and roughening of a flat graphite substrate is directly visualized at the nanoscale by scanning probe and electron microscopy. The etching damage in graphite and the properties of the exfoliated sheets are compared by Raman spectroscopy and X-ray diffraction analysis. The results show the trade-off between exfoliation speed and preservation of graphene quality. A key step to achieve efficient exfoliation is to couple gas production and mechanical exfoliation on a macroscale with non-covalent exfoliation and preservation of graphene properties on a molecular scale.**

## 1. Introduction

As a one-atom-thin carbon sheet, graphene has been intensively studied due to its impressive mechanical, thermal, optical and electronic properties. High-quality monolayers of graphene can be obtained on wafer scale by chemical vapor deposition or epitaxial growth. Though, massive production of graphene on ton scale, possibly with eco-friendly techniques, will be needed to allow good processability and low costs applications in composites, batteries, inks, etc.

Luckily, Nature has provided us with large amounts of high-quality graphene sheets, stacked inside mineral graphite; all we need to find is a convenient way to efficiently exfoliate it into single sheets, preserving its nice conjugated honeycomb structure. To do this, we should overcome the non-covalent, weak but significant interactions present between graphene sheets (≈43 meV/atom).[1] Furthermore, to exploit the high surface area of graphene as a substrate for catalysis, sensing, hydrogen or charge storage, a thorough understanding of the exfoliation mechanisms of graphene in liquids is needed.

Nowadays, graphite can be exfoliated by different chemical methods in liquid phase. One of the simplest approaches to disperse graphene sheets is ultrasonic treatment in organic solvents. Some dipolar aprotic solvents (e.g., *N*,*N*′-dimethylformamide (DMF) or *N*-methylpyrrolidone (NMP)) or surfactants in aqueous solutions revealed to be effective to stabilize graphene in solution without re-aggregation.[2,3] The mechanism of graphene dispersion in these solvent is not definitively clear on a molecular scale and flake dimensions are mostly below 1 μm.[2,4]

A more effective but disruptive approach to solubilize graphene is by covalent modification, in particular by the formation of graphene oxide (GO). In presence of strong oxidants, the aromatic carbon network is oxidized with the creation of hydroxyl, carboxyl and epoxy moieties.[5] The hydrophilic nature of these moieties on GO facilitates the solution processing of highly concentrated single sheets on different substrates.[6] The GO sheets can be then reduced back to give conductive reduced graphene oxide (rGO), to be used in working microelectronic devices.[7,8] However, numerous defects on GO are not fully restored after reduction and the electronic properties of rGO are poorer compared to those of the pristine graphene.

Another more controllable, slightly less disruptive approach to exfoliate graphite takes advantage of electrochemistry. By adjusting the driving potential in suitable electrolytes, graphite electrodes can be either negatively or positively intercalated to give graphene intercalation compounds (GICs), and then exfoliated by solvent decomposition directly during electrochemical treatment or by further thermal treatment.[9]

Dr. Z. Y. Xia, Dr. E. Treossi, Dr. A. Zanelli, Dr. V. Palermo
Istituto per la Sintesi Organica e la Fotoreattività - Consiglio Nazionale delle Ricerche
via Gobetti 101, 40129 Bologna, Italy
E-mail: palermo@isof.cnr.it
S. Pezzini, Dr. V. Bellani
Dipartimento di Fisica and CNISM
Universitá degli Studi di Pavia
via Bassi 6, 27100 Pavia, Italy
Dr. E. Treossi
Laboratorio MIST.E-R Bologna
via Gobetti 101, 40129 Bologna, Italy
Dr. G. Giambastiani
Istituto di Chimica dei Composti OrganoMetallici - Ricerche and Consorzio INSTM
via Madonna del Piano 10, 50019 Sesto Fiorentino, Italy
Dr. F. Corticelli, Dr. V. Morandi
Istituto per la Microelettronica e Microsistemi
Consiglio Nazionale delle Ricerche
via Gobetti 101, 40129 Bologna, Italy

**DOI: 10.1002/adfm.201203686**

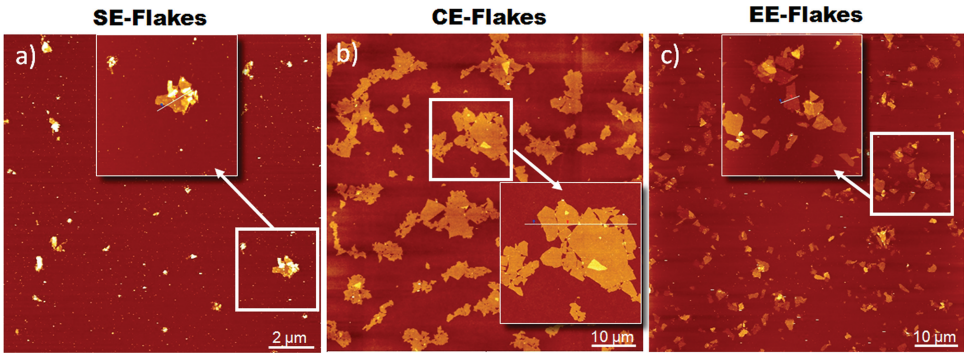


**Figure 1.** AFM image of soluble flakes obtained by a) sonication-assisted exfoliation-SE, b) chemical exfoliation-CE and c) electrochemical exfoliation-EE. The flakes have been spin coated on SiOx/Si from solution. The insets show a zoom-in taken in the white square areas. Height profiles taken along the white lines in the insets are shown in the Supporting Information, Figure S13. Z-range: (a) and inset of (a) 20 nm; (b) and inset of (b) 5 nm; (c) and inset of (c) 15 nm.

Even if some of these techniques have been intensively studied in recent years,[10] a comprehensive comparison of the different exfoliation mechanisms is still needed. The commonly accepted rational about graphene exfoliation is (roughly) that the more defects are introduced in the lattice, the more soluble are the sheets, the more efficient is the exfoliation. Sheet solubility is for sure fundamental to stabilize graphene in solution; however, the exfoliation process itself is a complex phenomenon that takes place on nanometer and mesoscopic scales and, in analogy to other solubilization processes,[11] will depend on a complex competition between chemical, electrostatic and van der Waals interactions, as well as fluid dynamics on the microscale. The final result will always depend not only on thermodynamics, but on kinetic factors as well. A clear evidence of this is that, even if the single GO sheets are highly hydrophilic, dry powders of GO often need intense sonication to be exfoliated in water.

Typical studies on graphite exfoliation mechanism focus on the solubilized sheets obtained during the exfoliation. Usually, they use graphite powder or flakes as starting material and then analyze the obtained sheets by Raman spectroscopy, to quantify defect density and exfoliation grade, and different microscopy techniques to measure sheets' size and thickness distribution.[4] A table summarizing the results obtained in different exfoliation studies is available in Supporting Information. This approach, although highly effective in quantifying the exfoliation efficiency, can hardly give useful information on the exfoliation mechanism that generates the different types of graphene and graphene oxide.

Here, we present a different approach to the study of graphite exfoliation by the above techniques. We analyze not only the graphene successfully dispersed, but focus our attention on the graphite that is left behind after the exfoliation process.

For this, rather than using graphite powder or microscopic flakes, we choose as starting substrate the flat surface of highly oriented pyrolytic graphite (HOPG).

In this way, the surface exfoliation process can be easily followed by optical microscopy (OM), atomic force microscopy (AFM) and scanning electron microscopy (SEM). X-rays diffraction (XRD) and Raman spectroscopy are also used to monitor substrate damage on atomic scale, and the effectiveness of the intercalation process. The electrochemical exfoliation process is also characterized by cyclic voltammetry (CV).

The exfoliated sheets, once dispersed in solution, are re-deposited as single sheets to be analyzed by AFM, or re-stacked in thick layers and studied again by AFM, XRD and Raman.

Following the changes in morphology and roughness of the HOPG surface on the proper scale, we observe the similarities and differences in mechanisms that lead to exfoliation, and how effectively they can be used to produce highly exfoliated graphene sheets.

## 2. Results

**Figure 1** shows the typical sheets obtained by sonication assisted exfoliation (SE) in DMF, chemical exfoliation (CE) by Hummers method and electrochemical exfoliation (EE) in diluted sulfuric acid. AFM profiles of the sheets are also reported in SI. Details on the preparation of each sample are reported in the experimental section at the end of this paper. It is evident that sheet lateral size of different flakes obtained varies greatly among the different techniques, decreasing in the following order: CE-HOPG (≈10 μm) > EE-HOPG (≈1 μm) > SE-HOPG (several hundred nm), and the result is consistent with the numerous works published on each exfoliation technique (a table summarizing some published works on the topic is reported in Supporting Information, Figure S1). Sonication in DMF, being the only technique among the three that does not involve covalent modification, yields very small flakes with several thick aggregates. Chemical oxidation yields the sheets with larger lateral size that, in agreement with previous results, can be processed without any significant aggregation, and deposited on substrates being nearly 100% monolayers.[6,7] The sheets exfoliated by chemical oxidation have a uniform thickness of ca. 1 nm, typical of chemically exfoliated GO, in agreement with previous results.[7]

Electrochemical exfoliation yields sheets with a smaller lateral size respect to chemical oxidation and larger thickness, with the presence of several bi- and multilayers.

While the differences observed in the exfoliated sheets can be easily attributed to the different amount of chemical damage

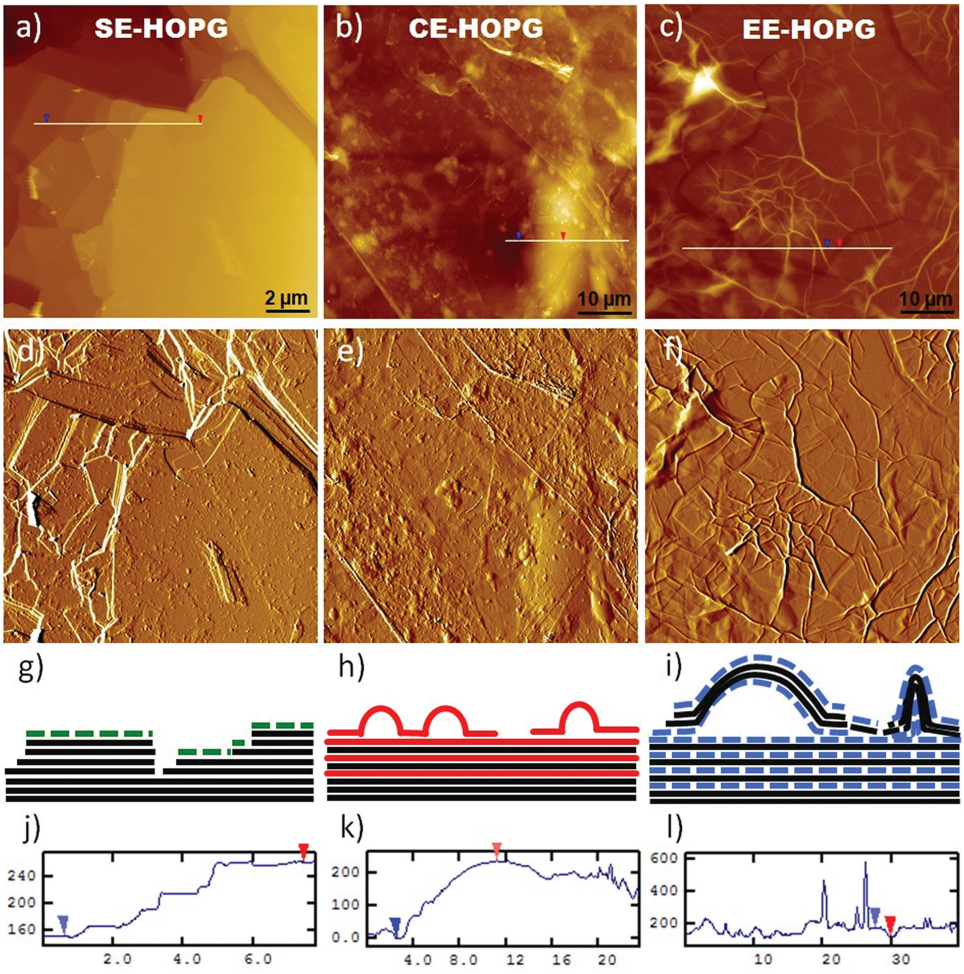


**Figure 2.** AFM images of HOPG basal surface after treatment by a) sonication-assisted (SE-HOPG), b) chemical (CE-HOPG) and c) electrochemical (EE-HOPG) exfoliation of HOPG. Z-range: a) 400 nm, b) 600 nm, c) 1 µm. d–f) Gradient-filtered version of each image. g–i) Schematic representation of the structure of the HOPG substrate after exfoliation procedures. j–l) Height profiles taken along the lines shown in (a–c).

of the sheets, the exact exfoliation mechanism can be understood only by watching at the graphite substrates from where the sheets have been exfoliated.

**Figure 2**a–c shows AFM images of the HOPG substrate remaining after partial removal of graphene sheets by the three liquid exfoliation techniques. In order to show all fine details of the surface, the corresponding gradient-filtered images are reported as well (Figure 2d–f). The difference between the three processes is clearly visible also in the AFM profiles shown in the insets below each image and schematized in the cartoons in Figure 2g–i, where dashed or colored lines indicate the different kind of damage or intercalation of the sheets.

SE yields a surface similar to original graphite, with the presence of larger steps and higher roughness. CE exfoliation gives roughness on nano- and microscale, with the formation of small and large rounded areas raised above the substrate, i.e., blisters due to sub-surface gas production. EE yields as well blister formation, and presence of a large amount of ripples due to surface cracking, blister explosion and macroscopic deformation of the surface.

Each process will be described in better detail in the following sections, before directly comparing the three processes.

### 2.1. Sonication Assisted Exfoliation in Organic Solvent

HOPG surface has been exfoliated by sonication in DMF, a typical method used to obtain sheets of non-defective graphene.[2,4]

The effect of the sonication time on the amount of material dispersed, the size of the exfoliated sheets and the fraction of graphene monolayers obtained have already been the subject of a systematic and comprehensive study,[4] and will not be discussed here; we will focus on the effect of sonication on the macroscopic graphite. SE graphite (Figure 2a) is quite similar to original graphite, with flat areas and straight steps. However, tens of nanometer high steps are observed on the surface, and the root mean square (RMS) roughness increases with exfoliation time, due to the removal of small fragments induced by sonication. Different snapshots of the evolution of HOPG

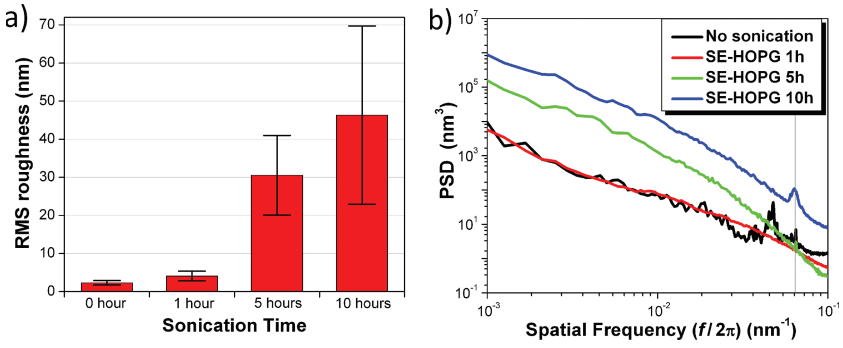


**Figure 3.** a) Evolution of RMS roughness of SE-HOPG in DMF for different times (for each time bar, we collected at least 12 AFM images with 15 μm × 15 μm size). b) Evolution of power spectrum density (PSD) of SE-HOPG in DMF for different times.

morphology with sonication are reported in Supporting Information Figure S2; the increase of RMS roughness with sonication time, as measured by AFM on different areas of the sample, is shown in **Figure 3**a.

The leading process for sonication assisted exfoliation is a surface removal of material that leaves flat terraces similar to the ones observed in the pristine HOPG. There is no visible deformation of the graphite structure, and absence of mechanically deformed areas. Raman, visible absorption and FT-IR analysis do not show evidence of extensive chemical damage of the HOPG substrate (**Figure 4**a, Supporting Information Figure S3): only a very low-intensity D band develops at 1330 $cm^{-1}$ in the Raman spectrum. On the other hand, the Raman signature of exfoliated flakes (black line in Figure 4a) show intense D and D′ (1617 $cm^{-1}$) bands, respectively related to short and long range type disorder.

It is known that the D-band originates from inter-valley double resonance processes, due to very short-range disorder potentials (e.g., adatoms, vacancies, defects),[12] while D′-band originates from intra-valley double resonance processes induced by long-range disorder (ripples, dislocations or charged impurities). The small size of the flakes (100–500 nm) relative to the size of the Raman probe (5 μm) may influence this result as a consequence of large edge-scattering contribution.[13]

The exfoliation mechanism of the surface is evident by following the increase of the RMS roughness of the substrate, as measured by AFM (Figure 3a). While maintaining local flatness on the 1–10 nm scale, the substrate is eroded into flat terraces having typical size of hundredths of nm, and depth of tens of nm. In this case, the exfoliation process is very superficial and slow; exfoliation and substrate roughening become relevant only after several hours of sonication. This latter point is confirmed by power spectrum density analysis (PSD); this is a Fourier-based, surface analysis tool that allows quantifying surface roughness on different spatial frequencies ($f$) in reciprocal space, corresponding to different length scales ($\lambda$) in real space. PSD is calculated as the angular average of the squared Fourier transform of a surface (form a more detailed description of the technique see ref.[14]). Figure 3b shows the PSD of graphite substrates after different sonication times in DMF, obtained by averaging the PSD of different AFM images. In this case, the PSD gives the roughness on length scales ($\lambda = 2\pi/f$) ranging roughly form 10 to 1000 nm. No significant roughening is observed on small and large scale even after 1 h sonication; for longer sonication time, an initial roughening on $\lambda > 16$ nm ($f < 0.4$ $nm^{-1}$) is observed, then followed by a general roughening increase on all length scales.

XRD analysis of the SE-HOPG substrates after exfoliation (**Figure 5**a) confirms that SE does not affect the graphite bulk in depth. Among the flakes exfoliated by SE, there is a low yield of few-layer sheets, while most of the material is composed of thick fragments.

### 2.2. Chemical Exfoliation

The chemical exfoliation (CE) of HOPG has been performed by a modified Hummers' method (for details see ref.[6]).

Samples prepared at four different oxidation times (10 s, 60 s, 10 min and 30 min) are characterized by optical microscopy, AFM and Raman spectra. Optical microscopy and AFM images of CE-HOPG show the formation of irregular blisters (**Figure 6**). After just 10 s of treatment we observe a large amount of blisters formed on the surface. Additional blisters and wrinkles appear for 60 s treatment. For longer oxidation time (10 min and 30 min), further growth and merging of blisters is clearly observed.

AFM measurements show also in better detail the formation of the blisters with a diameter of few μm and height up to 400 nm (Figure 6e–h). Blisters present both rounded and irregular, elongated shapes, likely due to the presence of local defects (steps, highly oxidized regions) that favor directional layer exfoliation and blister growth in specific directions (Figure 6a). In some cases, preferential exfoliation along defects is so strong to follow steps on the surface, yielding a network of raised ridges that run along the surface (Figure 6f).

Even if blisters often have irregular shapes, we observe (by an extensive statistical analysis of AFM images) that the blisters' shape changes during oxidation. **Figure 7** shows the ratio between blister radius $L$ and height $h$, measured by AFM (for the irregular blisters, we have always measured the lateral dimension in the narrower part). More than 220 blisters have been measured for the initial stages of oxidation (t = 10 s and t = 60 s). While $L$ and $h$ vary on a large range of sizes, their ratio $\delta$ ($\delta = L/h$) is fairly constant, and different for the two different samples. The contact angle $x$ of the blister between the blister edge and the plane can be calculated from $h$ and $L$ values (see Supporting Information Figure S4 for details):

$$\sin x = \frac{2hL}{L^2 + h^2} = \frac{2\delta}{\delta^2 + 1} \quad (1)$$

Initial oxidation stages (t = 10 s) give blisters that have small radius size ($L < 450$ nm) but high $h$ values (up to 350 nm), thus having a high curvature radius and a high contact angle $x$ = 79° ± 12° ($\delta$ = 1.21 ± 0.20). The blister growth is not always stable, especially in the first stages of exfoliation, as suggested by the presence of "relaxed" blisters, having large $L$, low $h$, and

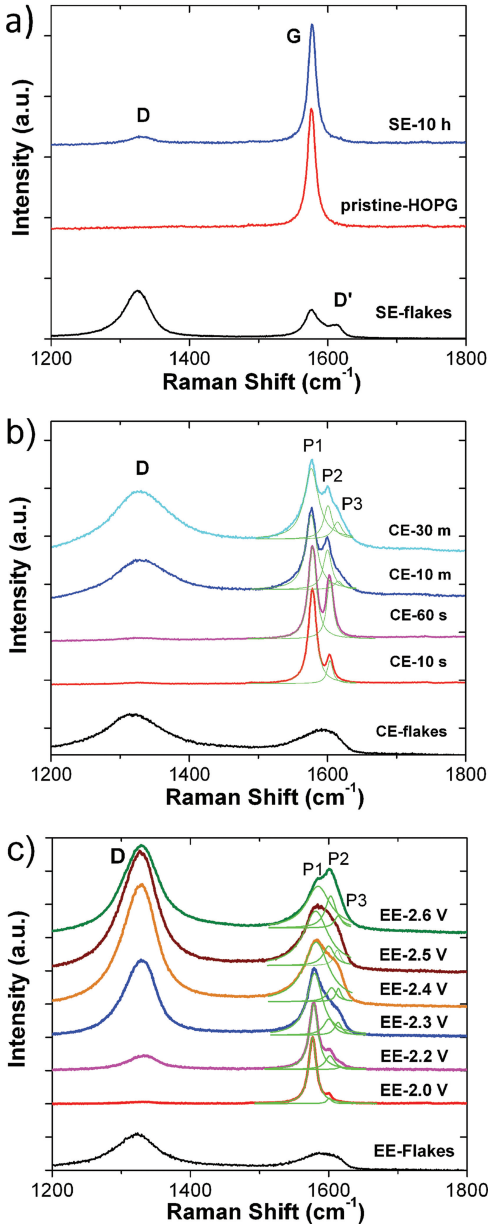


**Figure 4.** Raman analysis of a) graphite sonicated in DMF for 10 h; b) graphite chemically exfoliated at different times; and c) graphite electrochemically exfoliated at different voltages. Each image shows the spectra measured on the solid HOPG (colored lines) and on the solubilized flakes (black line below).

irregular $\delta$ (black points in Figure 7 with $h < 100$ nm). Their shape can be due to gas leakage, or more likely to a relaxation of the graphite sheets, which detach due to pressure, increasing blister width and reducing blister height.

After 60 s of treatment, the size of all blisters has changed significantly, with a general relaxation of blister structure, increase in $L$ and decrease in $h$ (Figure 7). The blisters' contact angle decreases to $x = 14° \pm 0.5°$ ($\delta = 7.92 \pm 0.22$), suggesting a larger delamination of the graphite upper-layers to reduce internal pressure.[15] For longer treatment times (10 min and 30 min), irregular blisters and wrinkles cover most of the HOPG surface with an increase of surface roughness, and statistical analysis of blisters is not possible.

Samples exfoliated by chemical oxidation show a complex Raman signal (Figure 4b), with multiple peaks structure in the G-band zone.

Initially, only the typical G peak due to in-plane $E_{2g}$ optical phonon mode of graphite is observed at 1577 $cm^{-1}$; upon oxidation, this peak decreases, while two other peaks at 1600 $cm^{-1}$ and 1617 $cm^{-1}$ appear and grow in time. To avoid any ambiguity, in Figure 4 we number P1, P2, P3 the peaks at 1577 $cm^{-1}$, 1600 $cm^{-1}$ and 1617 $cm^{-1}$ respectively.

The P1 and P2 peaks are attributed to two different $E_{2g}$ due to the C-C stretching mode of atoms composing the sheets in bulk graphite and atoms in the sheets adjacent to the intercalated layer. P1 is due to the inner, non-intercalated graphite layers ($E_{2g2}(i)$ mode), while P2 is due to the bounding graphite layers, adjacent to $HSO_4^-$ intercalants ($E_{2g2}(b)$ mode).[16]

The intensity ratio of the P1 and P2 peaks can be related to the intercalation stage index $n$ by means of $P2/P1 = \sigma_i/\sigma_b * (n\text{-}2)/2$,[17] where $\sigma_i/\sigma_b$ (assumed equal to 1) is the ratio of the cross-section of Raman scattering from interior and bounding layers. The intercalation stage index extracted from the spectra in Figure 4b decreases from $n \approx 8$ (10 s) to $n \approx 5$ (60 s) increasing with treatment time (**Figure 8**a shows an evolution of each peak with treatment time). For longer times (10 min, 30 min) there is no increase of the intercalation but rather a slight decrease, likely due to exfoliation of the superficial intercalated layers, while a strong broadening of the bands due to deep chemical oxidation is observed. Raman signal P3 instead could be identified with the previously mentioned D′ band (not completely resolved from the broadened G-band in these measurements), which is caused by large scale damage and deformation of the substrate induced by oxidation.[16,18]

The Raman spectra of exfoliated flakes of CE (black line in Figure 4b) are comparable to the ones previously obtained on chemically exfoliated GO. For instance the FWHM of the D peak of the CE-flakes (Figure 4b) is ≈110 $cm^{-1}$, to be compared with ≈110 $cm^{-1}$ of GO we measured in one of previous works,[7] ≈110 $cm^{-1}$ measured in ref.[19] and ≈130 $cm^{-1}$ measured in ref.[20] Also the relative intensity of the D peak with respect to the one of G peak observed in the present sample is comparable with what observed in the abovementioned references.

### 2.3. Electrochemical Exfoliation

HOPG samples have been partially exfoliated in 0.5 M $H_2SO_4$ solution by applying increasing voltages. The electrochemical exfoliation has two main effects: i) the bulk graphite swells macroscopically, due to electrolyte intercalation and decomposition, producing gas and creating a highly expanded structure, and ii) exfoliated material is detached from the bulk solid due to the gas eruption, and dispersed in solution.

**Figure 9** shows OM and AFM images of a typical exfoliation process as observed at different times and relatively high bias on the same sample, which help understanding how large amounts of materials are detached from the substrate. Even

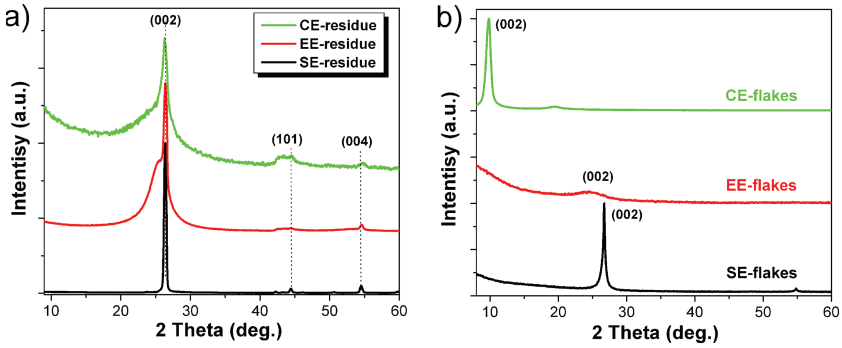


**Figure 5.** XRD patterns of a) the residual HOPG samples and b) the exfoliated sheets, successfully transferred in solution. The flakes were then re-stacked in thick layers by drop-casting on quartz, to obtain a measurable XRD signal. All the spectra are normalized on the 002 peak, except the spectra of EE-flakes in (b).

in this case the exfoliation proceeds by gas production and blister formation, but the speed and scale of the process are larger than what observed in CE. Relevant blister formation is observed even after few-seconds treatment when sufficient voltage is applied; the blisters have a large size, up to several tens of μm, and tend to cluster together; the gas formation process is so strong to deform the upper layers, which bend upward, and form a network of cracks visible by OM and by AFM (Figure 9d,h). The blisters grow continuously upon explosion or gas release, then collapse forming the network of ripples visible on the surface by AFM.

The exfoliation is effective enough to be visible by naked eye even after a few minutes treatment. The stacked graphite sheets swell due to visible gas formation and bubbling, yielding expanded structures that resemble (on a macroscopic scale) open books (Supporting Information Figure S11a,b); on a microscopic scale a foam-like structure is instead observed (Supporting Information Figure S12). The increase of sample volume can be relevant, creating highly expanded sheets that have a volume more than 40 times the original volume (Supporting Information Figure S11b). The amount of material released in solution is also relevant, and makes the solution dark (Supporting Information Figure S11c).

The microscopic structure of the exfoliated HOPG, as analyzed by SEM, shows clearly the effect of the treatment, with large sheets of multi-layer graphene having ≈100 nm thickness (Supporting Information Figure S12 and Figure S5).

The expanded sheets are at distance of many μm apart, and form a self-standing, robust structure with pretty high surface area. Even if it is not possible to measure precisely the sheet thickness, we have measured a specific surface area (SSA) of 6.6 $m^2$ $g^{-1}$; this is about three orders of magnitude higher than the surface area of the original HOPG material (in good agreement with the increase of active surface observed by voltammetry, see below), but still orders of magnitude lower than the maximal theoretical area achievable by perfect exfoliation of graphene (2600 $m^2$ $g^{-1}$), indicating that bulk exfoliation has acted mostly on a mesoscopic scale, and not at single sheets level. From the ratio between measured and theoretical surface area, an average thickness of ≈400 monolayers can be estimated for the material swelled, but still in solid phase.

OM and AFM observations of the EE-HOPG surface confirm the presence of blisters on all the samples exfoliated at potentials

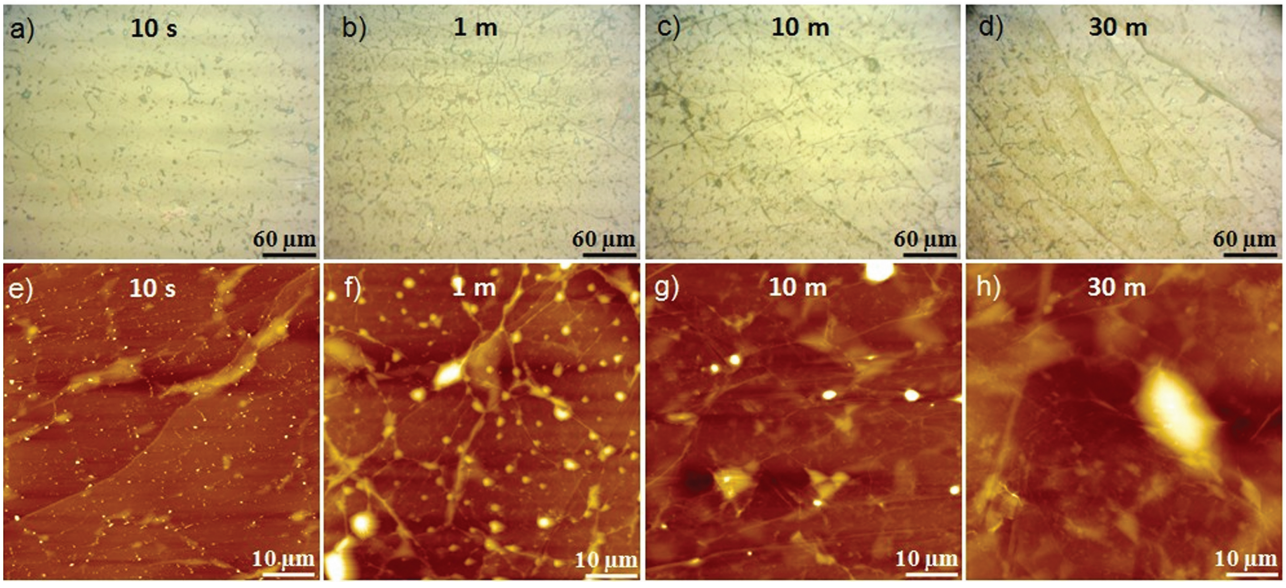


**Figure 6.** OM (a–d) and AFM (e–h) images of graphite chemically exfoliated at different reaction times: a,e) 10 s, b,f) 1 min, c,g) 10 min, d,h) 30 min. Z-ranges for images (e–h) are 350 nm, 350 nm, 400 nm, and 400 nm, respectively.

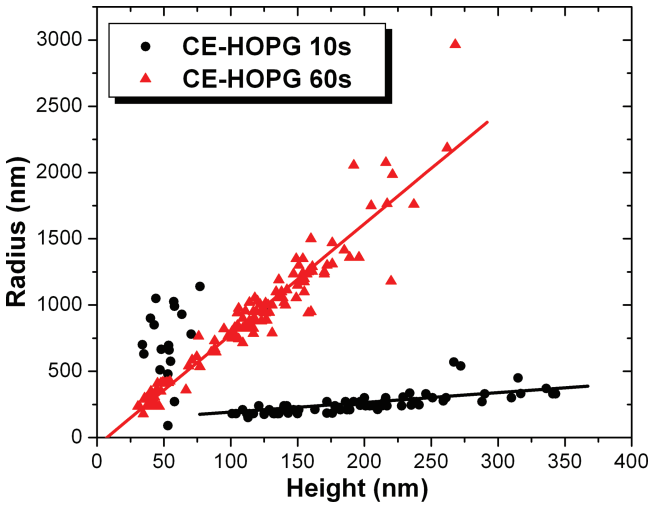


**Figure 7.** Statistical analysis of height and lateral size of blisters obtained by chemical exfoliation of graphite.

above 1.6 V (see also CV results here below and Supporting Information Figure S6). At low voltage, some blisters already appear on the EE-HOPG basal planes with average lateral size of 0.3–1.0 μm and height 10–100 nm; differently from CE samples, no constant height-width ratio is observed (statistics about 170 blisters from AFM images are shown in Supporting Information Figure S7). For 1.8 V bias, more blisters are visible in AFM and OM images. Many tiny blisters are observed around the step defects always present on the surface of HOPG indicating a preferential intercalation of the solvent in correspondence of sheet edges (Supporting Information Figure S6). It is known that blisters come from the intercalation of electrolyte and water into HOPG followed by subsurface gas evolution.[21] The intercalation process preferentially etches the step defects, grain boundaries and edge sites with weak van der Walls interactions and then yields gas production in correspondence of these sites.

Even if both CE and EE processes proceed through blister formation, the treated materials give significantly different results as analyzed by XRD and Raman.

EE-HOPG samples show evidence of the intercalation process. XRD data in Figure 5a, red line, show a sharp XRD peak due to inner, undamaged graphite and a broader peak due to the more disordered surface, which has been attacked by the treatment. This broad peak is slightly shifted towards smaller angles as compared to HOPG ($2\theta = 26°$ d = 0.35 nm), with a modest increase of the interlayer spacing and a strong increase of peak width due to the drastic reduction of crystal (domain) size. As comparison, CE-HOPG samples do not show this feature, even after long treatments time (Figure 5a, green line) indicating a more disordered, non periodic intercalation. Raman analysis gives an increasing P2 signal as well, confirming the intercalation process, together with a P3 signal indicative of disorder. Figure 4c and Supporting Information Figure S8 shows the evolution of P1, P2, P3 peaks for increasing exfoliation voltage. Figure 8b,c shows the evolution of P1, P2, P3 peaks in CE and EE samples respectively. P2 ratio increases with applied bias indicating a larger amount of intercalated layers on the HOPG surface.

A main advantage of the electrochemical exfoliation of HOPG compared to graphite powders is that the whole sample remains electrically connected; thus, after the expansion stage when exfoliation takes place on mesoscopic scale, the thin layer of graphene oxide formed on the surface of the exfoliated areas can be reduced back by simply applying a negative bias to the sample (Supporting Information Figure S9). Electrochemical expansion was investigated by monitoring the anodic current variation through electrochemical voltammetry. HOPG is stable up to 1.5 V vs SCE. The oxidation peak that occurs around 1.6 V may be attributed to the combination of the water electrolysis and graphite oxidation, consistent with previous works[15,21] (Supporting Information Figure S9a). The exfoliation process can also be followed in real time by chronoamperometric measurements. Supporting Information Figure S9b shows a typical response curve of HOPG upon exfoliation at 2.0 V; first, a steep increase of current is observed due to the increase of active surface area upon expansion, followed by a decrease indicative of predominant oxidation on the surface by side reactions (see also Raman measurements). The material obtained in this way has a relatively high surface area, and is stable upon voltage cycling, showing a current ≈500 times higher than the original HOPG samples (Figure 9d), in agreement with surface area measurements.

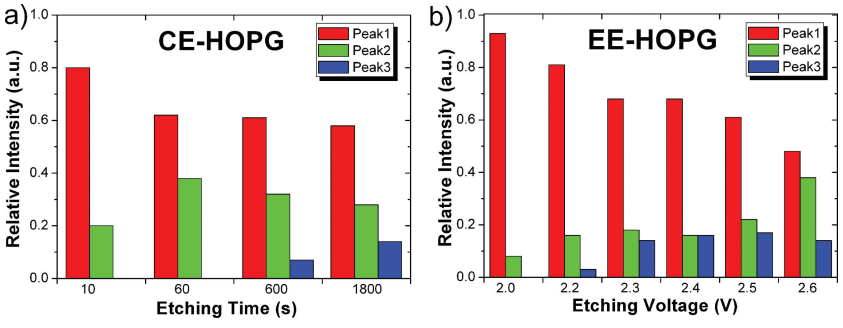


**Figure 8.** a) Evolution with increasing etching time of Raman P1, P2 and P3 peaks for CE-HOPG samples. b) Evolution with increasing applied bias of Raman P1, P2 and P3 peaks for EE-HOPG samples.

### 2.4. Comparison of the Exfoliation Processes and Discussion

We should underline that, in all the three studied processes, exfoliation is always promoted by some kind of mechanical action acting at the mesoscale. In SE the mechanical action arises from cavitation bubbles, with radius of hundreds of μm, which generate high strain rates in the surrounding liquid upon implosion.[3,22] However, AFM data (Figure 2 and Supporting Information Figure S2) show that these bubbles, being formed in the liquid phase, do not have

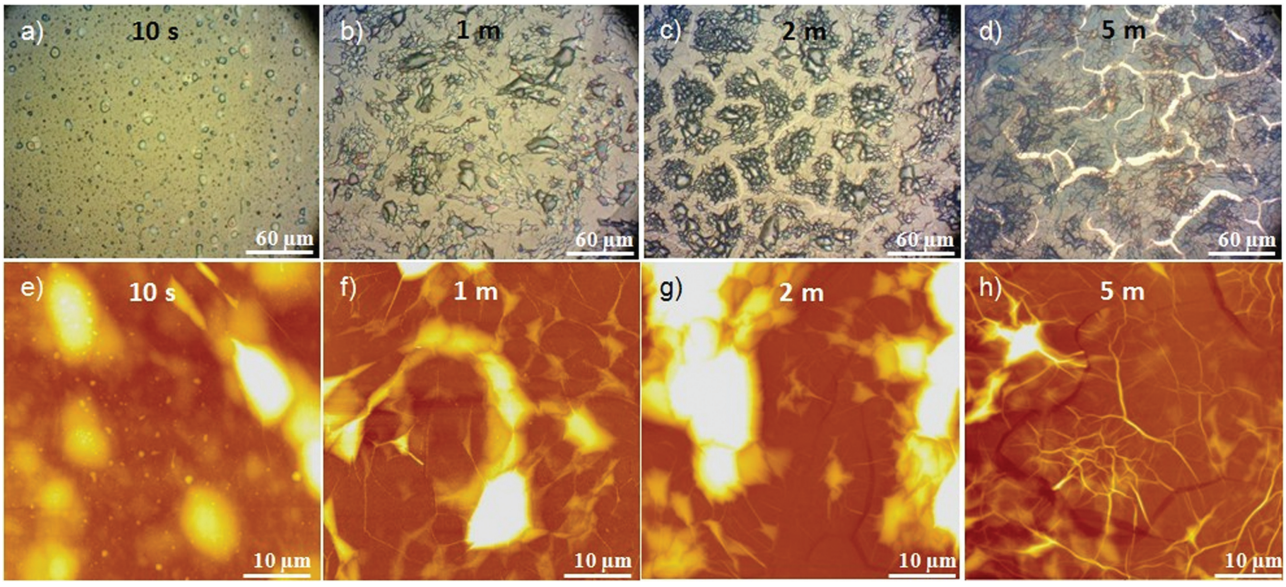


**Figure 9.** OM (a–d) and AFM (e–h) images of a graphite sample electrochemically exfoliated at 2.5 V for different reaction times: a,e) 10 s; b,f) 1 min, c,g) 2 min, d,h) 5 min. Z-range: e), f), h) 1.0 µm, g) 2.5 µm.

visible effects on the surface of sonicated graphite, where flat terraces morphology is maintained. The process induces minimal mechanical damage to graphite, but acts only on the very surface, thus it is pretty slow and shows visible effects (increase of roughness) only for sonication times of several hours (Figure 3).

SE treatment affects only the first few nm of the graphite substrate, and proceeds through removal of small graphitic fragments having size <1 µm (Figure 1a) from the exposed surface of graphite, with no action on the inner bulk, no mechanical expansion and no in-depth intercalation, thus requiring many hours of sonication to give low concentrations and small pieces of disordered graphene sheets in solution. Even if the dispersion of the sheets is thermodynamically favorable, the lack of mechanical expansion and the shallow penetration depth of the solvent molecules oblige to introduce in the system a lot of ultrasonic energy, so that the lateral size of the sheets is significantly reduced.[4]

In CE and EE treatment, mechanical exfoliation is also due to bubble formation, but the pressures come from inside the material. Both chemical and electrochemical oxidations proceed through unstable graphite intercalation compounds (GICs) as intermediate.[23]

$$C_p + HSO_4^- + yH_2O \rightleftharpoons C_p^+ \cdot HSO_4^- \cdot yH_2O + e^- \quad (2)$$

Then, main irreversible oxidative reactions[21] take place, such as graphite oxide formation:

$$C_p + HSO_4^- \xrightarrow[-H_2SO_4]{+H_2O} C_p^+ OH^- (sp^2) \longrightarrow C_p OH (sp^3) \quad (3)$$

electrochemical carbon dioxide formation:

$$C_p + 2H_2O \longrightarrow C_{p-1} + CO_2 + 4H^+ + 4e^- \quad (4)$$

or chemical carbon dioxide formation:

$$5C_p + 2Mn_2O_7 + 8H^+ \longrightarrow 5C_{p-1} + 5CO_2 + 4Mn^{2+} + 4H_2O \quad (5)$$

in case of the electrochemical process, water electrolysis also takes place, with more gas generation:

$$2H_2O \longrightarrow O_2 + 4H^+ + 4e^- \quad (6)$$

The chemical oxidation process is an aggressive way to destroy graphite crystallites. After reversible chemical intercalation step, oxidation in CE is performed by the strong oxidant $Mn_2O_7$ created in solution by the reaction of potassium permanganate with sulfuric acid.[24]

Intercalation and gas production are therefore important factors favoring exfoliation; though, the amount of damage they introduce in graphene lattice could in principle be very small.[15] Mechanical exfoliation does not need extensive graphite oxidation, or disruption of material conjugation. A mesoscopic blister 1 µm wide by 100 nm high can be generated by oxidizing only 0.02% of the carbon atoms within the blister footprint in electrochemical way.[21]

The pressure generated between the graphene layers by these reactions can be very high. For chemically exfoliated GO single sheet, the separation pressure to overcome Van der Waals force is 25 bar,[25] while for single graphene sheets the encapsulated pressure is as high as 720 bar. In the case of multilayer sheets, the pressure could be even much higher, over several thousands bar.[21] With such a high pressure, the generated forces in the form of blisters can elastically deform the graphene multilayers, and even erupt from deep inside graphite to rip several-hundred layers mechanically forming large area blisters of elastically deformed graphene multilayers on the graphite surface, hundreds of nm high and tens of µm wide.[21]

Both electrochemical and chemical oxidation under harsh conditions (high voltage or strong oxidant) give efficient exfoliation, with dissolution of macroscopic amounts of material

and high yield of few-layer sheets in solution (see Figure 1 and ref.[7]). The process can readily expand bulk amounts of graphite, increasing the amount of substrate in contact with the solution, thus allowing dispersion of large quantities of material in short times.

Once transferred in solution, the graphitic material obtained with the three processes has different size and quality. We have performed XRD analysis of the exfoliated sheets, after re-stacking them in thick layers by drop-casting from solution on quartz, to obtain a material similar to GO paper, which gives a measurable XRD signal (Figure 5b). The re-deposited thick films prepared from the three types of sheets are clearly different from each other, as seen also by AFM (Supporting Information Figure S10).

CE-flakes are fully oxidized and re-stack with no graphitic peaks, only two peaks ($2\theta_1 = 9.6°$, $2\theta_2 = 18°$) that are typical first and second order of the interlayer distance of GO, corresponding to layer distance of 0.92 nm. In EE flakes, the (002) refection of the $\pi$–$\pi$ stacked layers is slightly shifted towards smaller angles ($2\theta = 22°$) with a slightly increased graphene interlayer distance of 0.41 nm, and the intensity is much weaker than the original HOPG, suggesting the drastic reduction of crystal (domain) size. SE flakes show the typical diffraction peak of graphite, not due to re-stacking of single sheets, but rather to the strong signal coming from graphite like multilayers.

Overall, we see that exfoliation by sonication in DMF proceeds on a layer-by-layer basis; only the upper part of the HOPG is interested, and the process is slow, requiring several hours to have visible effects on the substrate roughness. Electrochemical exfoliation proceeds by mechanical expansion due to gas formation. Whole areas of the substrate rise up due to gas formation, tearing apart the superficial layers and removing large amounts of material. The process acts in depth in the material, and readily expands even bulk amounts of HOPG up to 40 times their initial volume. Damage to HOPG is relevant and proportional to the applied bias, with disruption of crystalline stacking. Exfoliation is fast and relatively efficient, yielding many mono- and bi-layers, which do not re-stack efficiently.

CE is the most damaging treatment for HOPG, destroying significantly the crystalline layer through deformation and intercalation; though, the process acts on a smaller scale as compared to EE, oxidizing the upper layers of the HOPG substrate with less cracking and swelling on macroscopic scale; the obtained sheets are mostly monolayers, highly soluble, which tend to re-stack giving a more uniform, layered material.

The ideal technique to exfoliate graphene would need to act with different driving forces on different length scales; first, using mechanical exfoliation on mesoscopic scale to penetrate in depth in the material, with minimal damage of graphene sheets, possibly using gas production reactions that do not involve removal of carbon atoms. This expansion step should be coupled or followed by exfoliation on molecular scale by surfactants or suitable solvents, exploiting supramolecular interactions, to avoid damage of graphene.

## 3. Conclusions

We have studied the most common liquid phase exfoliation methods of graphene from bulk graphite. By using a macroscopic HOPG crystal as starting material, it is possible to study the structure of both the exfoliated and the non-exfoliated fractions on nanometric and mesoscopic scale. Among the three methods, chemical oxidation is a very effective but disruptive way to exfoliate graphite. Electrochemical oxidation allows a fast exfoliation and in depth disruption of bulk quantities of graphite, but does anyhow yield defective graphene. Sonication in organic solvents gives graphene of best quality, but acts only on the uppermost few nanometers of the surface, requiring thus long treatment times.

The differences observed between the three methods show very well the existing trade-off between speed and efficiency of exfoliation on one side, and preservation of the material quality on the other. A key step to develop efficient exfoliation will be to couple gas production, mechanical exfoliation on macro-scale with non-covalent exfoliation and preservation of graphene chemistry on molecular scale.

## 4. Experimental Section

*Materials*: HOPG (12 mm × 12 mm × 2 mm, Grade ZYH) was purchased from GE Advanced Ceramics and cut into thin pieces of size 12 mm × 12 mm × 0.3 mm. Potassium permanganate (Sigma-Aldrich, 99%), sodium nitrate (Sigma-Aldrich, 99%) and sulfuric acid (Sigma-Aldrich, 95–97%) were used for the oxidation of HOPG surface. *N,N*-Dimethylformamide (Sigma, 99%) was used as solvent in ultrasonication procedures.

*Sonication of HOPG in DMF*: HOPG flakes dispersed in DMF (10 mL) were sonicated in a water bath (Elmasonic P 70 H, 37kHz, 220 W) for different times (1 h, 5 h and 10 h). After each period, the sonication exfoliated sample (SE-HOPG) surface was analyzed by AFM to check the morphology changes. After 10 h, the DMF solution containing the exfoliated sheets was centrifuged.

*Chemical Exfoliation of HOPG without Electric Potential*: The HOPG was chemically exfoliated by using a modified Hummers method, as previously described.[6] Different geometries were used to expose to the solution only the flat surface of the HOPG or the edges as well.

The HOPG sample was cleaved with an adhesive paper tape and fixed onto a glass Petri-dish. For the flat-side-only oxidation process, a drop of the oxidizing solution (prepared from 10 mL of sulfuric acid, 0.1 g of sodium nitrate, and 0.6 g of potassium permanganate)[6] was deposited onto the HOPG surfaces. The reaction was run on different samples with different reaction times: 10 s, 1 min, 10 min and 30 min, respectively. Then, the oxidized samples (CE-HOPG) were rinsed with 5 wt% $H_2SO_4$ and 1 wt% $H_2O_2$ mixture, 5 wt% HCl and deionized (DI) water respectively, then blow-dried with dry nitrogen for 2 min.

Using a macroscopic HOPG crystal instead of graphite powder the surface exposed to the solvent is much lower; the exfoliation yield is also much lower. Large amounts of CE flakes in high concentration were thus obtained by keeping HOPG samples in the oxidizing solution for 5 days without stirring, and then treating the sample as previously described. Here, the much longer time is to guarantee comparable amounts of dispersed flakes after reaction.[6]

*Electrochemical Expansion and Exfoliation of HOPG*: The surface of HOPG samples was cleaved with scotch tape before each experiment, to have a clean starting surface, and connected to a metallic clamp. Then, half of the graphite was immersed into a proper solution (vide infra). An Au wire was used as counter-electrode with an electrode separation of 1 cm. The ionic solution was prepared by taking 4.8 g of sulfuric acid and diluted in 100 mL of DI water ($c \approx 0.5$ M). The electrochemical exfoliation process was carried out for 0.5 hours by applying DC bias on graphite electrode at potentials ranging from 0 V to + 2.6 V. After reaction, the electrochemically exfoliated graphite samples (EE-HOPG) were washed with DI water several times and blow-dried with dry nitrogen for 2 min.

Solutions of electrochemically expanded sheets were produced by electrochemical treatment under 3.5 V for 0.5 h, and then purified by filtration and repeated washing with DI water. After drying, these particles were re-dispersed in DMF solution, mildly sonicated for 10 min to disperse large aggregates and then spin coated on silicon substrates for analysis.

*Voltammetry Study of Electrochemical Exfoliation of HOPG*: Cyclic voltammetry studies (CV) were carried out in water (Milli RO 15 Water Purification System, 0.56 μS $cm^{-1}$) 0.5 mol $L^{-1}$ $H_2SO_4$ with an AMEL 5000 electrochemical system. The working electrode was HOPG. The reference electrode was aqueous Saturated Calomel Electrode (SCE), and the auxiliary electrode was Pt wire separated from the working electrode by a glass frit.

*Characterization*: AFM measurements were carried out using a Digital Instruments AFM (NT-MDT), Nanoprobe cantilevers (Model: RTESP, Material: 1-10 Ohm-cm Phosphorus (n) doped Si, f0: 27-309 kHz, k: 20-80 N/m; from Veeco) operating in tapping mode. Optical microscopy (OM) images were measured by Optech Technology microscopy. The SEM images were obtained with a ZEISS 1530 instrument. XRD measurements were collected with a PANalytical X'PertPro instrument in Bragg-Brentano reflection mode ($\lambda$ = 0.1542 nm, X'Celerator detector). IR data were acquired on a Perkin-Elmer Spectrum BX FT-IR system. Raman scattering measurements were carried out with a micro-Raman spectrometer (Model: LabRAM from Horiba Jobin-Yvon), using a 50 × objective (laser spot diameter ≈ 5 μm), laser excitation wavelength of 632.8 nm and laser power ~ 4 mW.

The BET specific surface area (SSA) and porosity (the latter based on BJH method) were measured on an ASAP 2020 Micromeritics instrument, using $N_2$ as absorbent at the liquid $N_2$ temperature (77 K). Before measurements, the EE-HOPG sample (98 mg) was degassed at 403.15 K for 24 h.

## Supporting Information

Supporting Information is available from the Wiley Online Library or from the author.

## Acknowledgements

The authors wish to thank Dr. M. Gazzano for XRD data collection and fruitful discussion. This work was supported by the European Science Foundation (ESF) under the EUROCORES Program EuroGRAPHENE (GOSPEL), the Operative Program FESR 2007-2013 of Regione Emilia-Romagna–Attività I.1.1. and the EC Marie-Curie ITN-GENIUS (PITN-GA-2010-264694).

Received: December 13, 2012
Published online: April 17, 2013

[1] a) R. Zacharia, H. Ulbricht, T. Hertel, *Phys. Rev. B* **2004**, *69*, 155406; b) S. Lebegue, J. Harl, T. Gould, J. G. Angyan, G. Kresse, J. F. Dobson, *Phys. Rev. Lett.* **2010**, *105*, 196401; c) D. S. Li, W. Windl, N. P. Padture, *Adv. Mater.* **2009**, *21*, 1243.

[2] Y. Hernandez, M. Lotya, D. Rickard, S. D. Bergin, J. N. Coleman, *Langmuir* **2010**, *26*, 3208.

[3] U. Khan, H. Porwal, A. O'Neill, K. Nawaz, P. May, J. N. Coleman, *Langmuir* **2011**, *27*, 9077.

[4] U. Khan, A. O'Neill, M. Lotya, S. De, J. N. Coleman, *Small* **2010**, *6*, 864.

[5] a) A. Lerf, H. Y. He, M. Forster, J. Klinowski, *J. Phys. Chem. B* **1998**, *102*, 4477; b) A. Bagri, C. Mattevi, M. Acik, Y. J. Chabal, M. Chhowalla, V. B. Shenoy, *Nat. Chem.* **2010**, *2*, 581; c) M. Quintana, A. Montellano, A. E. D. Castillo, G. Van Tendeloo, C. Bittencourt, M. Prato, *Chem. Commun.* **2011**, *47*, 9330; d) M. Quintana, K. Spyrou, M. Grzelczak, W. R. Browne, P. Rudolf, M. Prato, *ACS Nano* **2010**, *4*, 3527.

[6] E. Treossi, M. Melucci, A. Liscio, M. Gazzano, P. Samori, V. Palermo, *J. Am. Chem. Soc.* **2009**, *131*, 15576.

[7] A. Liscio, G. P. Veronese, E. Treossi, F. Suriano, F. Rossella, V. Bellani, R. Rizzoli, P. Samori, V. Palermo, *J. Mater. Chem.* **2011**, *21*, 2924.

[8] a) J. M. Mativetsky, E. Treossi, E. Orgiu, M. Melucci, G. P. Veronese, P. Samori, V. Palermo, *J. Am. Chem. Soc.* **2010**, *132*, 14130; b) J. M. Mativetsky, A. Liscio, E. Treossi, E. Orgiu, A. Zanelli, P. Samori, V. Palermo, *J. Am. Chem. Soc.* **2011**, *133*, 14320.

[9] C. Y. Su, A. Y. Lu, Y. P. Xu, F. R. Chen, A. N. Khlobystov, L. J. Li, *ACS Nano* **2011**, *5*, 2332.

[10] X. Li, G. Zhang, X. Bai, X. Sun, X. Wang, E. Wang, H. Dai, *Nat. Nanotechnol.* **2008**, *3*, 538.

[11] V. Palermo, P. Samori, *Angew. Chem. Int. Ed.* **2007**, *46*, 4428.

[12] A. C. Ferrari, *Solid State Commun.* **2007**, *143*, 47.

[13] A. C. Ferrari, J. C. Meyer, V. Scardaci, C. Casiraghi, M. Lazzeri, F. Mauri, S. Piscanec, D. Jiang, K. S. Novoselov, S. Roth, A. K. Geim, *Phys. Rev. Lett.* **2006**, *97*, 187401.

[14] V. Palermo, D. Jones, *Mater. Sci. Semicond. Process.* **2001**, *4*, 437.

[15] D. C. Alsmeyer, R. L. McCreery, *Anal. Chem.* **1992**, *64*, 1528.

[16] M. S. Dresselhaus, G. Dresselhaus, *Adv. Phys.* **2002**, *51*, 1.

[17] S. Solin, *Graphene Intercalation Compounds*, Springer-Verlag, Berlin **1990**.

[18] L. J. Hardwick, M. Hahn, P. Ruch, M. Holzapfel, W. Scheifele, H. Buqa, F. Krumeich, P. Novak, R. Kotz, *Electrochim. Acta* **2006**, *52*, 675.

[19] G. Eda, M. Chhowalla, *Adv. Mater. 22*, 2392.

[20] S. Stankovich, D. A. Dikin, R. D. Piner, K. A. Kohlhaas, A. Kleinhammes, Y. Jia, Y. Wu, S. T. Nguyen, R. S. Ruoff, *Carbon* **2007**, *45*, 1558.

[21] C. A. Goss, J. C. Brumfield, E. A. Irene, R. W. Murray, *Anal. Chem.* **1993**, *65*, 1378.

[22] F. Hennrich, R. Krupke, K. Arnold, J. A. R. Stutz, S. Lebedkin, T. Koch, T. Schimmel, M. M. Kappes, *J. Phys. Chem. B* **2007**, *111*, 1932.

[23] a) J. Fiang, F. Beck, *Carbon* **1992**, *30*, 223; b) V. V. Avdeev, L. A. Monyakina, I. V. Nikolskaya, N. E. Sorokina, K. N. Semenenko, *Carbon* **1992**, *30*, 819.

[24] D. R. Dreyer, S. Park, C. W. Bielawski, R. S. Ruoff, *Chem. Soc. Rev.* **2010**, *39*, 228.

[25] M. J. McAllister, J. L. Li, D. H. Adamson, H. C. Schniepp, A. A. Abdala, J. Liu, M. Herrera-Alonso, D. L. Milius, R. Car, R. K. Prud'homme, I. A. Aksay, *Chem. Mater.* **2007**, *19*, 4396.